ACS OMEGA

http://pubs.acs.org/journal/acsodf

Article

Preparation and Characterization of an Invasive Plant-Derived Biochar-Supported Nano-Sized Lanthanum Composite and Its Application in Phosphate Capture from Aqueous Media

Enmin Zong, Yuanyuan Shen, Jiayao Yang, Xiaohuan Liu,* and Pingan Song*

Cite This: *ACS Omega* 2023, 8, 14177−14189

Read Online

ACCESS | Metrics & More | Article Recommendations | Supporting Information

ABSTRACT: Invasive plants pose a great threat to natural ecosystems owing to their rapid propagation and spreading ability in nature. Herein, a typical invasive plant, *Solidago canadensis*, was chosen as a novel feedstock for the preparation of nano-sized lanthanum-loaded *S. canadensis*-derived biochar (SCBC-La), and its adsorption performance for phosphate removal was evaluated by batch adsorption experiment. The composite was characterized by multiple techniques. Effects of parameters, such as the initial concentration of phosphate, time, pH, coexisting ions, and ionic strength, were studied on the phosphate removal. Adsorption kinetics and isotherms showed that SCBC-La shows a faster adsorption rate at a low concentration and SCBC-La exhibits good La utilization efficiency than some of the reported La-modified adsorbents. Phosphate can be effectively removed over a relatively wide pH of 3−9 because of the high pH_{pzc} of SCBC-La. Furthermore, the SCBC-La shows a strong anti-interference capability in terms of pH value, coexisting ions, and ionic strength, exhibiting a highly selective capacity for phosphate removal. Additionally, Fourier transform infrared spectroscopy (FT-IR) and X-ray photoelectron spectroscopy (XPS) measurements reveal that hydroxyl groups on the surface of SCBC-La were replaced by phosphate and manifest the reversible transformation between $La(OH)_3$ and $LaPO_4$. Considering its high adsorption capacity and excellent selectivity, SCBC-La is a promising material for preventing eutrophication. This work gives a new method of pollution control with waste treatment since the invasive plant (*S. canadensis*) is converted into biochar-based nanocomposite for effective removal of phosphate to mitigate eutrophication.

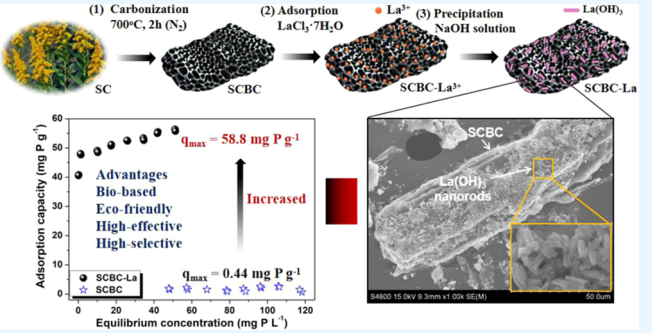

1. INTRODUCTION

With the rapid development of industrial and agricultural sectors, water bodies around the world increasingly suffer varying degrees of pollution,[1−10] among which phosphorus pollution has attracted increasing attention.[3,11−14] Phosphorus, as an indispensable nutritive substance on the earth, is beneficial to the normal growth of all living organisms.[15−18] However, excessive discharge of phosphate (PO_4^{3-}) to water bodies can accelerate eutrophication, leading to undesirable blue algae blooming, water quality worsening, and potential threats to human health.[19] Based on the data available in the literature,[20,21] total phosphorous can vary from 8.5 mg L^{-1} in landfill leachate to 740 mg L^{-1} in fresh urine. The United States Environmental Protection Agency (USEPA) stipulates that the maximum concentration of phosphate ions in discharged wastewater should be less than 0.05 mg L^{-1}. Thus, it is urgent to develop efficient methods to remove excess phosphate before discharging it into water. To this end, tremendous efforts have been devoted to improving phosphate removal by using adsorbents because of their ease of operation, low cost, and high efficiency. Last years have witnessed the sequential development of various PO_4^{3-} adsorption materials, including waste materials (e.g., lignin), synthetic metal oxides and hydroxides (e.g., aluminum oxide hydroxide), and functionalized materials (e.g., metal−organic frameworks).[22−27] These adsorbents exhibit high adsorption performance for PO_4^{3-} removal; nevertheless, sustainable cost-effective biomass-derived adsorbents are still needed for this field of application.

Biochar, a low-cost carbon-rich material, has been usually produced by carbonizing biomass under oxygen-limiting conditions and exhibits great potential to remove contaminants from water owing to its abundant availability of sources, cost-effectiveness, environmental friendliness, and easy-availability features. To date, many kinds of biochar have demonstrated excellent capabilities to remove antibiotics,[28] dyes,[29] and metal ions.[30] Unfortunately, their PO_4^{3-} removal efficiency remains

Received: February 14, 2023
Accepted: March 27, 2023
Published: April 5, 2023

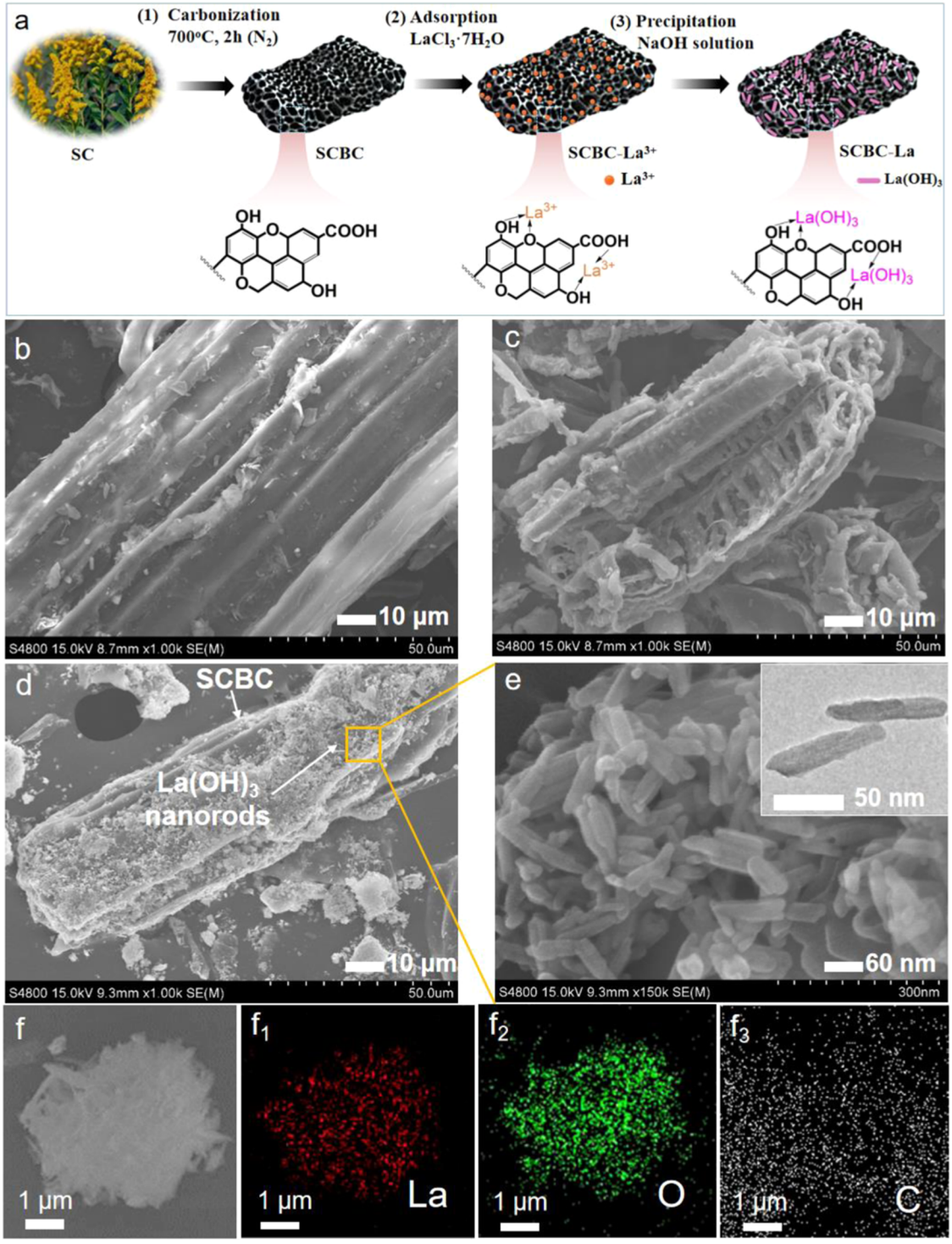

Figure 1. (a) Schematic procedure for the fabrication of nanocomposite adsorbent SCBC-La; SEM micrographs for (b) SC, (c) SCBC, and (d, e) SCBC-La; (f) SEM image of SCBC-La and its energy-dispersive X-ray spectroscopy (EDS) map scanning of (f_1) La, (f_2) O, and (f_3) C.

far unsatisfactory. The low PO_4^{3-} capturing capacity of biochar is mainly attributed to the abundant negatively charged functional groups on the biochar surface.[31] Loading metal-(hydro) oxides onto biochar has recently been used as a method to enhance their adsorption capacities toward PO_4^{3-}.[32] Among these metal(hydro) oxides, lanthanum (hydro) oxides exhibit superior advantages, such as high stability, low toxicity, and biocompatibility.[33,34] Furthermore, the nanocomposites containing lanthanum (hydro) oxides have been regarded as promising candidates for PO_4^{3-} removal due to their superior adsorption capacity, excellent adsorption selectivity, high removal efficiency, and wide operating pH range.[24,35,36] The interactions of precipitation, ligand exchange, and complexation are predominantly responsible for the adsorption process by La composites.[31]

Nowadays, *Solidago canadensis* has been extensively distributed in most provinces of China and is listed as one of the most destructive and widespread invasive plants.[37] This

https://doi.org/10.1021/acsomega.3c00992
ACS Omega 2023, 8, 14177−14189

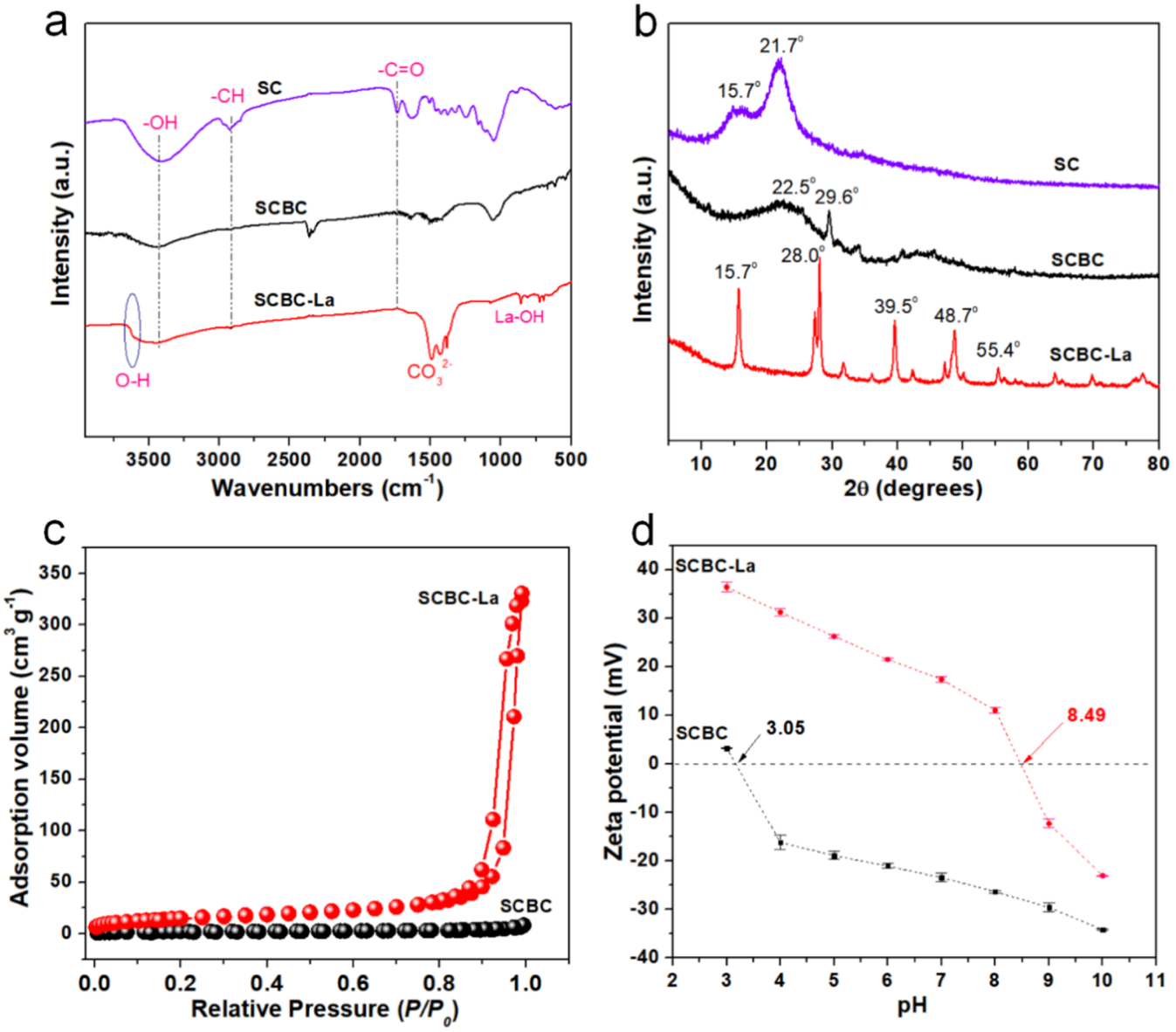

Figure 2. (a) FT-IR spectra and (b) XRD spectra for SC, SCBC, SCBC-La, and $La(OH)_3$, and (c) N_2 adsorption−desorption isotherms and (d) pH dependence for the ζ potentials of SCBC and SCBC-La.

invasive plant has harmful impacts on the native environment and the security of human life.[38−41] The abundant availability of invasive plants allows the massive production of *S. canadensis*-derived biochar, which can also provide a viable and economic approach to effectively control this invasive plant.[42−45] The adsorption of phosphate by modified biochar prepared from *S. canadensis* in the post-treatment process has not been studied extensively. Therefore, *S. canadensis* was used in this study to prepare biochar (SCBC). The SCBC was used to create lanthanum-modified biochar (SCBC-La) by coprecipitation with nano-sized $La(OH)_3$ particles. The decoration of $La(OH)_3$ into *S. canadensis*-derived biochar not only can significantly enhance the adsorption capacity of phosphate but also can open up an innovative approach to extending the applications of *S. canadensis*. Thus, the effects of phosphate removal by the La-based adsorbent using *S. canadensis*-derived biochar as the support would be necessary to unveil.

The objective of the present study was to fabricate a novel and cost-effective *S. canadensis*-derived biochar-based nano-lanthanum (hydro) oxides (SCBC-La) by a facile approach. The oxygen atoms present in biochar can bind lanthanum atoms through coordination (Figure 1a), indicating that $La(OH)_3$ nanoparticles can be stably deposited on the biochar surface. It also indicates that two components should have good thermodynamic compatibility.[46−48] The general physicochemical properties of SCBC and SCBC-La were extensively characterized by Fourier transform infrared spectroscopy (FT-IR), X-ray photoelectron spectroscopy (XPS), scanning electron microscope (SEM), transmission electron microscopy (TEM), X-ray diffraction (XRD), Brunauer−Emmett−Teller (BET), and ζ-potential. Various experiments were carried out to determine the adsorption isotherms and kinetics of the SCBC-La composite and the influences of coexisting anions, pH, and ionic strength on its phosphate adsorption. Moreover, the structural changes on the SCBC-La composite during the adsorption process were demonstrated to

https://doi.org/10.1021/acsomega.3c00992
ACS Omega 2023, 8, 14177−14189

Table 1. Physicochemical Features of SCBC and SCBC-La

samples	S_{BET} (m^2 g^{-1})	d (nm)	V_p (cm^3 g^{-1})	pH_{pzc}	C (%)	O (%)	La (%)
SCBC	8.02	6.433	0.012	3.05	69.97	16.47	
SCBC-La	55.87	36.63	0.512	8.49	33.04	35.86	29.86

propose the adsorption mechanisms. This work has developed a cost-effective biochar-based adsorbent for phosphate removal and opens up an innovative approach to extending the applications of invasive plants.

2. RESULTS AND DISCUSSION

2.1. Material Preparation and Physiochemical Characterization. The facile fabrication process of the SCBC-La nanocomposite is schematically illustrated in Figure 1a. First, biochar was obtained by carbonization of *S. canadensis* under a N_2 atmosphere, and some negatively charged groups (such as −COOH) were created on the surface of *S. canadensis*-derived biochar (SCBC). After $LaCl_3$ was added into the suspension of SCBC, La^{3+} ions tend to attach to the SCBC surface through coordination, and $La(OH)_3$ nanorods were deposited on the SCBC surface *via* hydrolysis of La^{3+} ions. Upon filtration, $La(OH)_3$ nanoparticle-decorated SCBC assembled into the target nanocomposite adsorbent SCBC-La. The nanostructure of the SCBC-La was confirmed by SEM and TEM, as shown in Figure 1b−e. It can be seen that the surface of SC is relatively smooth (see Figure 1b), and SCBC clearly shows a porous structure (see Figure 1c). Importantly, the SCBC-La clearly exhibits a typical rod-like nanocrystallite structure (diameter: 10−20 nm; length: 60−100 nm) attached on the surface of the SCBC (see Figure 1d,e), which indicates the formation of $La(OH)_3$ nanorods, as also evidenced by TEM characterization (inserted in Figure 1e). The EDS map scanning (see Figure 1f,f_1−f_3) shows that the element La is homogeneously distributed in the resultant SCBC-La, which suggests well-dispersed $La(OH)_3$ nanorods on the surface of SCBC-La that can provide more active sites for phosphate removal.

FT-IR spectra were employed to characterize the structural change of SC after modification (see Figure 2a). It can be seen that the band at around 3413 cm^{-1} of the raw material SC is due to the stretching vibration of the −OH group. The stretching band appears at around 2924 cm^{-1} to the stretching vibration of C−H, which is mainly because of $-CH_2$ and $-CH_3$, and the peaks at 1741 cm^{-1} ascribed to the stretching vibration of C═O. After carbonization, the intensity of the adsorption band was reduced, which is in line with the result of other research using palm kernel shells.[49] As to SCBC-La, the two peaks at 3609 and 650 cm^{-1} after La loading onto SCBC are assigned to the stretching and bending O−H vibrations of $La(OH)_3$, respectively,[50] which is also confirmed by the spectrum of $La(OH)_3$. In addition, Figure 2b shows the XRD patterns of SC, SCBC, SCBC-La, and $La(OH)_3$. It can be found that two peaks appeared at the 2θ of 15.7 and 21.7° in SC ascribed to the cellulose crystallinity. After carbonization, SCBC shows a broad peak at around 22.5° ascribed to the aromatization and graphitization of biomass, and another peak at ∼29.6° attributed to sylvite.[31] In the XRD spectrum of SCBC-La, the diffraction peaks at 2θ = 15.7, 28.0, 39.5, 48.7, and 55.4 correspond to (100), (101), (201), (300), (211), and (112) crystal planes of $La(OH)_3$, which matches well with the database in JCPDS file (card no. 83-2034), suggesting the formation of $La(OH)_3$ nanorods,[50] which is further confirmed by the binding energy peak of La 3d in the XPS spectrum of SCBC-La (Figure S1). The specific surface areas for SCBC and SCBC-La are further determined by N_2 adsorption/desorption isotherms. As presented in Figure 2c and Table 1, the S_{BET} of SCBC-La increases by 6-fold to 55.87 m^2 g^{-1} and its V_p shows a 41.7-fold increase to 0.512 cm^3 g^{-1} as compared with that of the SCBC. The formation of the nanostructure created by $La(OH)_3$ nanorods results in an elevation in both S_{BET} and pore volume (V_p). The substantial increase in the surface area compared to SCBC is probably because of the heterogeneous precipitation of $La(OH)_3$ on the outer surface of the SCBC. According to the IUPAC classification, the SCBC-La is considered to be a type IV isotherm, indicative of the presence of an irregular mesoporous structure.[51] Besides, the average pore size (36.63 nm) of SCBC-La indicates the existence of mesopores. Furthermore, the potential of zero charge also plays an important role in the adsorption process.[52] As shown in Figure 2d and Table 1, as compared with SCBC (pH_{pzc} ∼ 3.05), SCBC-La shows a much higher pH_{pzc} of ∼8.49 due to the introduction of lanthanum, which means that its surface charge is strongly positive with a pH value as high as 8.49, whereas SCBC possesses a weakly positive ζ potential with a lower pH < 3.05. Such a high pH_{pzc} value makes nanocomposite SCBC-La an effective PO_4^{3-} adsorbent in a relatively wide pH range.

2.2. Adsorption Isotherm. Figure 3 illustrates the adsorption isotherms of PO_4^{3-} uptake by SC, SCBC, and SCBC-La at 25 °C. As shown, both SC and SCBC have a very low capability of adsorbing PO_4^{3-} because of negative charges on their surface (see Figure S2), which indicates that it is inappropriate to apply directly to remove phosphate for them. Upon the loading of $La(OH)_3$ nanorods, the resultant biochar-based nanocomposite adsorbent SCBC-La shows obvious adsorption capability for PO_4^{3-}. The adsorption efficiency of PO_4^{3-} by the SCBC-La is evaluated in an initial concentration range of 50−120 mg L^{-1} (see Figure S3). We show an

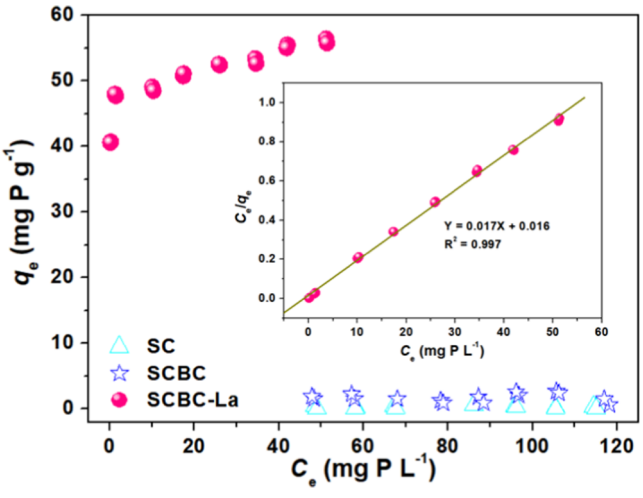

Figure 3. Phosphate adsorption isotherm for SC, SCBC, and SCBC-La. The inset shows the linear regression by fitting the equilibrium data with the Langmuir adsorption model.

https://doi.org/10.1021/acsomega.3c00992
ACS Omega 2023, 8, 14177−14189

Table 2. Equilibrium Parameters of Langmuir, Freundlich, and Temkin Isotherm Models

Langmuir isotherm			Freundlich isotherm			Temkin isotherm		
K_l (L mg^{-1})	q_m (mg g^{-1})	R^2	K_f (mg g^{-1})	n	R^2	A	B	R^2
1.06	58.8	0.997	46.11	24.39	0.784	0.784	45.485	0.9179

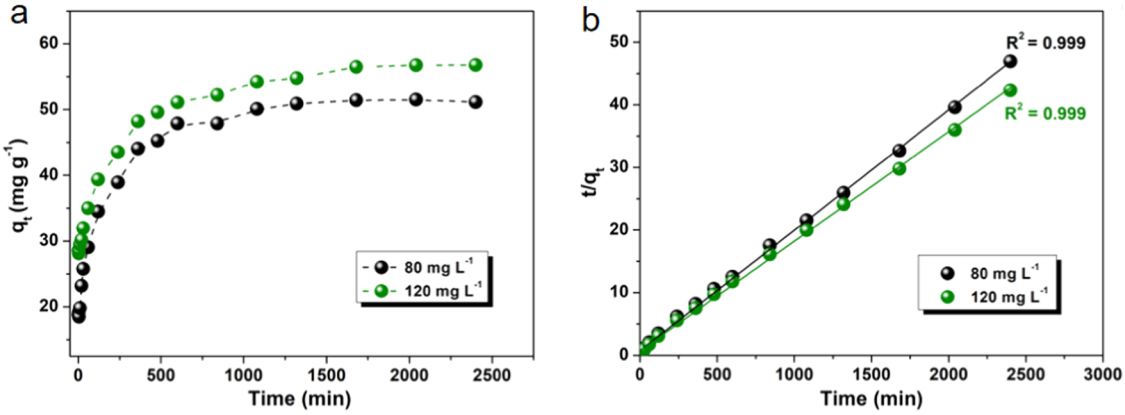

Figure 4. (a) Adsorption kinetics of phosphate on SCBC-La at two initial concentrations (80 and 120 mg L^{-1}) and (b) fitting results for pseudo-second-order models.

Table 3. Kinetic Parameters of Pseudo-First-Order and Pseudo-Second-Order Models for Phosphate Adsorption on SCBC-La

		pseudo-first-order kinetics			pseudo-second-order kinetics		
C_o (mg L^{-1})	($q_{e,exp}$)	($q_{e,cal}$) (mg g^{-1})	k_1 (g mg^{-1} min^{-1})	R^2	($q_{e,cal}$) (mg g^{-1})	k_2 (g mg^{-1} min^{-1})	R^2
80	51.1	31.3	0.002	0.705	52.6	0.0005	0.999
120	56.8	25.6	0.002	0.927	58.8	0.0004	0.999

adsorption efficiency as high as 98% when the initial PO_4^{3-} concentration is below 61 mg L^{-1}, giving rise to an adsorption capacity of 48 mg g^{-1}. A gradual decline in the PO_4^{3-} uptake efficiency is observed with increasing PO_4^{3-} concentration, but the adsorption capacity is enhanced to 56.4 mg g^{-1} when the initial PO_4^{3-} concentration is 120 mg L^{-1}. In order to study the adsorption isotherms, the following related formulas were used to investigate the Langmuir (eq 1), Freundlich (eq 2), and Temkin (eq 3) adsorption isotherm. The three equations can be expressed as

Langmuir model:

$$\frac{C_e}{q_e} = \frac{1}{q_m b} + \frac{C_e}{q_m} \quad (1)$$

Freundlich model:

$$\ln q_e = \ln K_f + \frac{1}{n} \ln C_e \quad (2)$$

Temkin model:

$$q_e = A + B \ln C_e \quad (3)$$

where q_e and q_m represent the amount of adsorbing phosphate per unit weight of the adsorbent at equilibrium and the maximum adsorption capacity (mg g^{-1}), respectively. C_e (mg L^{-1}), K_l (L mg^{-1}), and K_f (mg g^{-1}), respectively, refer to the equilibrium solution concentration, and n is the Freundlich empirical constant. A and B are the Temkin constants.

It is apparent that adsorption isotherm data are well fitted with the Langmuir adsorption model, showing a good linear relationship of C_e/q_e versus C_e (see Figure 3) with a high correlation coefficient of 0.997, as compared to that of the Freundlich isotherm model (0.784, see Figure S4 and Table 2) and Temkin isotherm model (0.9179, see Figure S5 and Table 2), indicating that the adsorption of PO_4^{3-} on SCBC-La is explained by the monolayer adsorption behavior.[33] Furthermore, the affinity between PO_4^{3-} and SCBC-La is further confirmed based on the Langmuir parameters using the separation factor R_L (eq S1). The R_L values of PO_4^{3-} adsorption by SCBC-La are determined to be 0.008 (between 0 and 1) when C_0 is the highest initial phosphate concentration in a solution of 120 mg L^{-1}, suggesting that PO_4^{3-} is favorably adsorbed by SCBC-La. Remarkably, SCBC-La is determined to display a capacity of 58.8 mg P g^{-1} according to the Langmuir model (see Table 2), which is 132 times higher than that of SCBC (0.44 mg P g^{-1}).

Furthermore, some lanthanum-containing adsorbents have been employed for the adsorption of phosphate,[31,33,34,53−58] as summarized in Table S1. SCBC-La simultaneously exhibits higher adsorption capacity (58.8 mg P g^{-1}) and La utilization efficiency (P/La = 0.90) than some of the reported La-incorporated materials. Such a high performance for phosphate removal is mainly attributed to the good dispersibility and exposure of $La(OH)_3$ nanorods on the surface of SCBC-La. In this regard, SCBC-La exhibited good competitiveness, indicating its potential application as a new-generation sustainable adsorbent for phosphate removal from wastewater.

2.3. Adsorption Kinetics. The adsorption kinetics is investigated by the real-time monitoring of the concentration change of PO_4^{3-} at fixed time intervals, as shown in Figure 4a. The phosphate adsorption process with the initial concentration of 80 mg L^{-1} is similar to that of 120 mg L^{-1}. It can be found that the adsorption amount of phosphate increases with increasing initial PO_4^{3-} concentration, and the adsorption

https://doi.org/10.1021/acsomega.3c00992
ACS Omega 2023, 8, 14177−14189

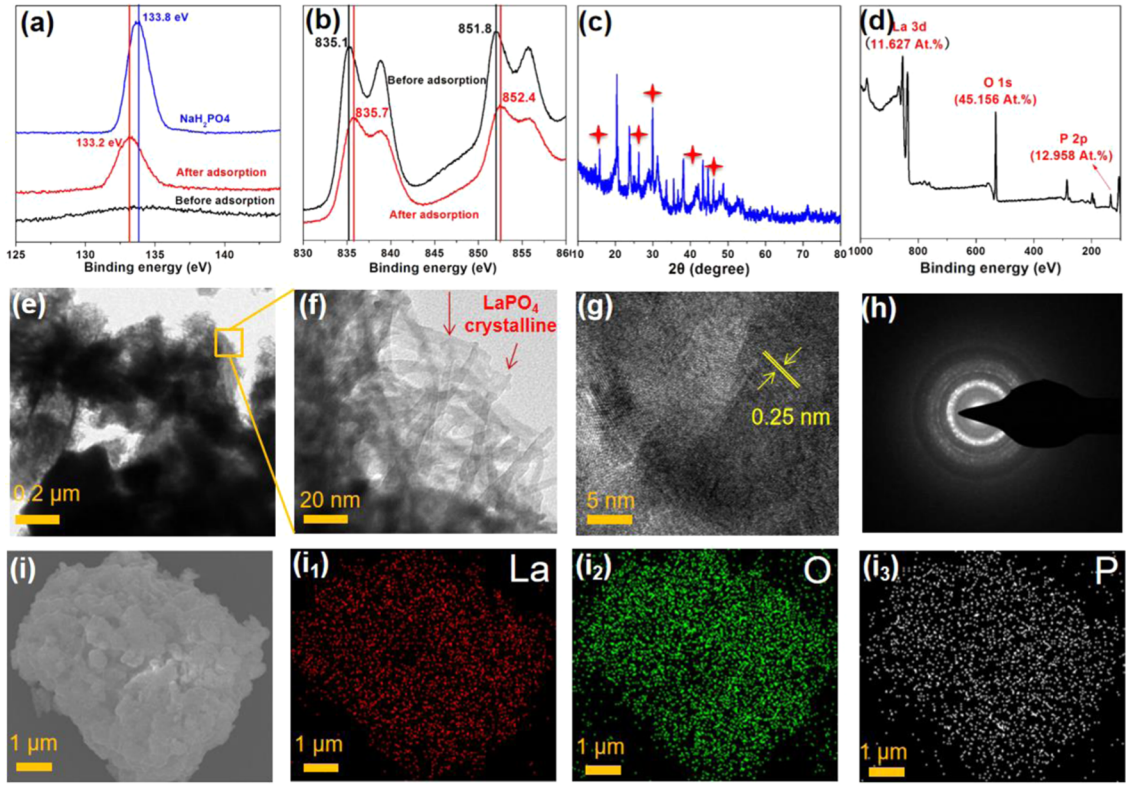

Figure 5. (a) FT-IR spectra and (b) XRD spectra of SCBC-La before and after phosphate adsorption; (c) XPS analysis of the P 2p spectrum; (d) XPS analysis of the La 3d spectrum; (e, f) TEM images; (g) HRTEM image; (h) selected-area electron diffraction (SAED) pattern of SCBC-La after phosphate adsorption; and (i) SEM image of SCBC-La after phosphate adsorption and its elemental distribution maps of (i_1) La, (i_2) O, and (i_3) P.

equilibrium time needs to be longer, which is consistent with our previous results.[25] The adsorption capacity of phosphate is determined to be 51.1 and 56.8 mg P g^{-1} and meanwhile the equilibrium is reached at about 1080 and 1680 min, respectively. Moreover, pseudo-first-order (eq S2) and pseudo-second-order (eq S3) adsorption models are generally used to further quantitatively analyze the adsorption kinetics.

The experimental data were fitted to the pseudo-first-order (see Figure S6) and the pseudo-second-order models (see Figure 4b). The kinetic parameters of PO_4^{3-} adsorption are summarized in Table 3. The pseudo-second-order model exhibits higher correlation coefficients (0.999 for 80 mg L^{-1} and 0.999 for 120 mg L^{-1}) relative to those of the pseudo-first-order model (0.705 for 80 mg L^{-1} and 0.927 for 120 mg L^{-1}), indicating that the adsorption data fitted well to the pseudo-second-order model. Moreover, their equilibrium adsorption capacities fitted by the pseudo-second-order model (52.6 mg g^{-1} for 80 mg L^{-1} and 58.8 mg g^{-1} for 120 mg L^{-1}) are close to the experimental results (51.1 mg g^{-1} for 80 mg L^{-1} and 56.8 mg g^{-1} for 120 mg L^{-1}). The results from the adsorption kinetics of PO_4^{3-} by SCBC-La in agreement with the pseudo-second-order model indicate a chemisorption behavior of the adsorption involving valence forces through the coordination or exchange of electrons between SCBC-La and PO_4^{3-}.[59]

2.4. Adsorption Mechanism. In order to understand the outstanding adsorption performance of PO_4^{3-} by SCBC-La, XPS, FT-IR, XRD, TEM, and SEM measurements are employed to investigate the binding interaction between the PO_4^{3-} and La species. The PO_4^{3-} inclusion within SCBC-La is verified by the appearance of the PO_4^{3-} signal at 133.2 eV attributed to the P 2p spectrum (see Figure 5a). The strong binding interaction between the PO_4^{3-} and La species in P@SCBC-La can be seen from the La 3d XPS spectrum, which exhibits a 0.6 eV blue shift for the PO_4^{3-} binding energy in P@SCBC-La as compared to that of SCBC-La (see Figure 5b). Moreover, the characteristic stretching mode of La-OH at 3609 cm^{-1} in the FT-IR spectrum of SCBC-La disappears upon saturation with PO_4^{3-}, confirming the interactions between La species groups and PO_4^{3-} (see Figure 6a). In addition, the XRD diffraction peaks of P@SCBC-La (see Figure 5c) indicate the complexation between PO_4^{3-} and La species and $LaPO_4$.[60,61] It is noteworthy that from the XPS results, the ratio of the atomic percentage of the La/P/O atomic ratio is 1.0:1.1:3.9 (Figure 5d), which is close to the theoretical value of $LaPO_4$ (1.0:1.0:4.0). The TEM images further confirm the formation of large numbers of needle-like crystalline $LaPO_4$ (see Figure 5e,f). Meanwhile, a high-resolution transmission electron microscopy (HRTEM) image reveals a lattice spacing of 0.25 nm on the basal planes, which matches well with the d-spacing of the (100) interplanar spacing for hexagonal $LaPO_4$ (see Figure 5g,h).[62] Additionally, the SEM-EDX mapping images (see Figure 5i,i_1−i_3) show homogeneous distribution of P throughout the sample particle, implying that PO_4^{3-} is present in the form of $LaPO_4$.[33]

Figure 6a illustrates the evolution of the chemical structure of SCBC-La in the adsorption−desorption process. The bands at 650 and 3609 cm^{-1} corresponding to La−O and −O−H stretching vibrations of $La(OH)_3$ can be seen in the fresh SCBC-La.[50] Upon saturation with PO_4^{3-}, the above bands almost disappear and two new peaks are clearly determined to appear at 615 and 539 cm^{-1} attributing to the O═P−O bending and O−P−O bending modes, respectively.[50] This

https://doi.org/10.1021/acsomega.3c00992
ACS Omega 2023, 8, 14177−14189

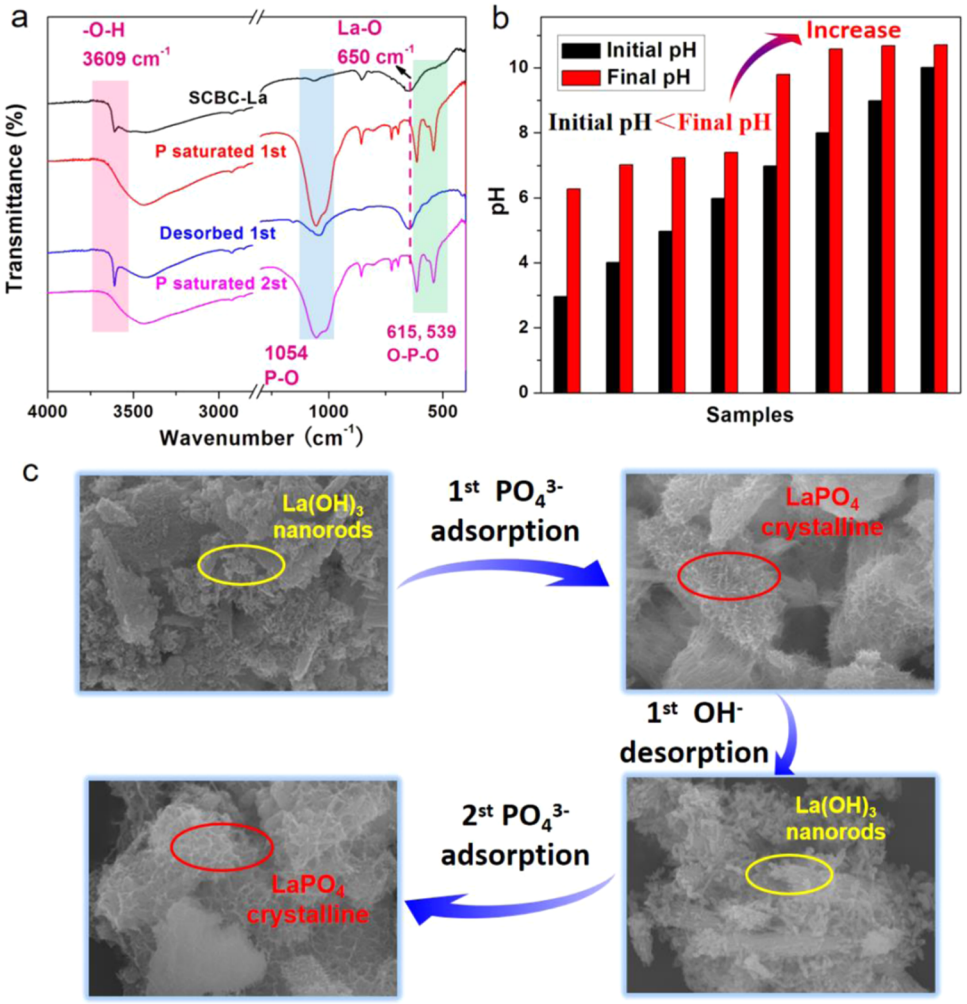

Figure 6. (a) FT-IR spectra of fresh SCBC-La, SCBC-La after first adsorption, SCBC-La after first desorption, and SCBC-La after second adsorption; (b) the changes of pH values before and after adsorption; and (c) SEM images of fresh SCBC-La, SCBC-La after first adsorption, SCBC-La after first desorption, and SCBC-La after second adsorption.

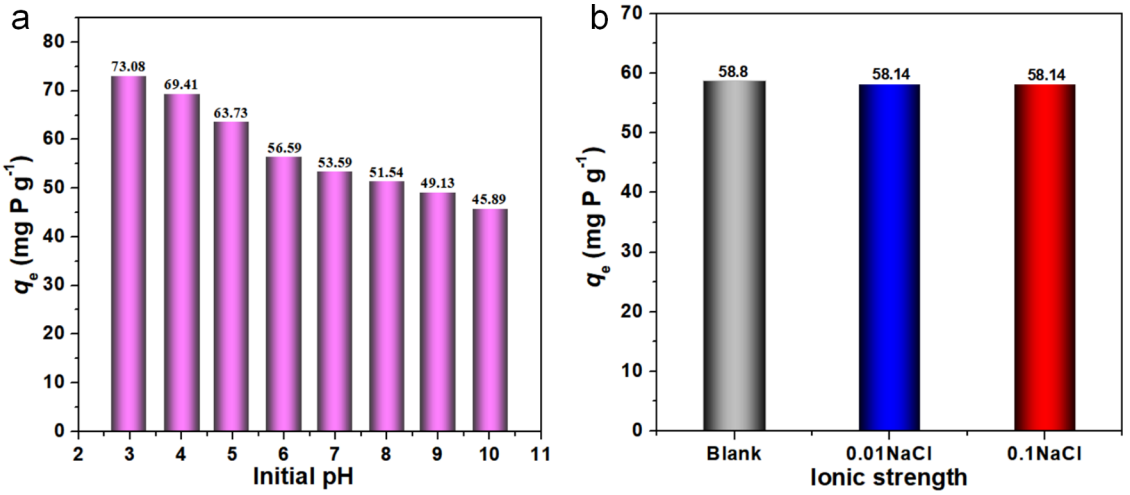

Figure 7. Effects of (a) the initial pH value and (b) ionic strength on phosphate adsorption of SCBC-La.

indicates that the −OH of La $(OH)_3$ is almost replaced by PO_4^{3-} during the adsorption, leading to the formation of $LaPO_4$ during PO_4^{3-} adsorption. Moreover, it is further evidenced by the increase in the final pH values at the adsorption equilibrium (final pH>initial pH) (see Figure 6b). Impressively, after desorption by NaOH solution, the La−O and −O−H stretching vibrations of $La(OH)_3$ can be readily recovered to the original state, and both the O═P−O bending and O−P−O bending modes completely vanish, indicating that $LaPO_4$ formed during adsorption transforms to $La(OH)_3$

https://doi.org/10.1021/acsomega.3c00992
ACS Omega 2023, 8, 14177−14189

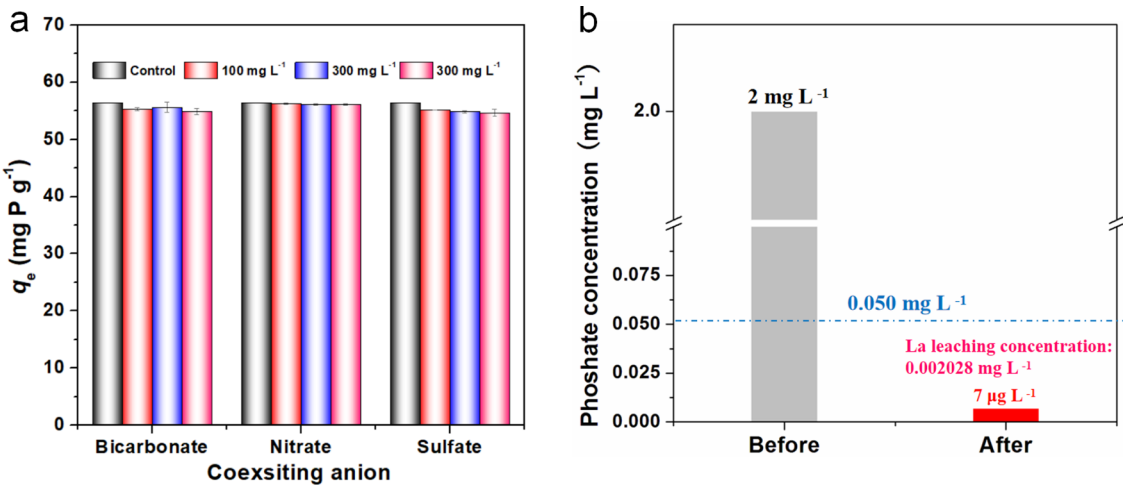

Figure 8. (a) Effect of coexisting anions on the adsorption capacity of SCBC-La for phosphate adsorption and (b) changes in the concentrations of phosphate in solution before and after 2 h treatment by SCBC-La.

through facile alkaline treatment, and simultaneously the adsorption capacity is recovered.[36] The evolution of the IR spectrum of SCBC-La during the second adsorption test is consistent with the first one, further manifesting the reversible transformation between $La(OH)_3$ and $LaPO_4$, as also evidenced by the changes of their morphologies (see Figure 6c).

2.5. Effect of pH and Ionic Strength on Phosphate Adsorption. The amount of phosphate retained by the adsorbents at different pH values is shown in Figure 7a. The phosphate adsorption decreases with increasing pH values, which is consistent with the results of our previous studies.[25,63] SCBC-La shows high PO_4^{3-} capture capacity of 73.08 mg g^{-1} at pH 3.0 and 53.59 mg g^{-1} at pH 7.0. Even in a slightly alkaline solution (a pH range of 7.0−9.0), the uptake amount of PO_4^{3-} can still reach more than 49.13 mg g^{-1}. SCBC-La exhibits the highest adsorption capacity of phosphate at pH = 3.0. It is mainly explained from the following two aspects: the zero point of charge (pH_{ZPC}) of SCBC-La and the phosphate species existing in water. The zero-point charge (pH_{zpc}) of SCBC-La is found to be 8.49 (Figure 2d). Consequently, the surface of SCBC-La is positively charged at a pH value of 3.0 in water. Additionally, the form of phosphate is dependent on the pH value of water and the pk_a of phosphate (pk_{a1} = 2.51; pk_{a2} = 7.20; pk_{a3} = 12.33) in aqueous solutions of various pH values. It can be seen that $H_2PO_4^-$ and HPO_4^{2-} are the dominant species when the solution pH ranges from 3.0 to 9.0. This clearly demonstrates that SCBC-La can effectively capture PO_4^{3-} under mildly acidic, neutral, and mildly alkali conditions in a wide pH range of 3.0−9.0. The adsorption capability of SCBC-La is superior to many previously reported adsorbents in terms of a wider pH range of conditions.

In addition, the effect of ionic strength on the adsorption of PO_4^{3-} onto SCBC-La is also elevated by adding different concentrations of NaCl (0.01 and 0.1 M) to the phosphate solution. The corresponding results are shown in Figure 7b. It can be found that the increasing NaCl concentrations from 0 to 0.01 and 0.1 M have not adversely affected the adsorption capacity of SCBC-La. This could be because of the lower affinity of Cl^- toward the adsorption sites on SCBC-La in comparison with PO_4^{3-}, and so there is no obvious competition between Cl^- and PO_4^{3-} during the process of adsorption. It is important to note that the complexation of the outer sphere will be generated if the adsorption of anions onto metal oxides is mainly dependent on ionic strength.[64] Thus, it can be concluded that the formation of inner-sphere complexation is an adsorption mechanism to SCBC-La when phosphate is adsorbed on SCBC-La.

2.6. Effect of Coexisting Anions on Phosphate Adsorption. It is of great significance to investigate the adsorption selectivity of adsorbents for practical application.[65] Adsorption selectivity of SCBC-La toward capturing PO_4^{3-} is evaluated by the addition of various coexisting anions of different concentrations (100, 200, and 300 mg L^{-1}) into the system of SCBC-La including bicarbonates (HCO_3^-), sulfates (SO_4^{2-}), and nitrates (NO_3^-), respectively. The corresponding results are shown in Figure 8a. Impressively, SCBC-La preserves over 96.9% of the original adsorption capacity of phosphate ions even under a high concentration of 300 mg L^{-1}, indicating that the coexisting anions nearly have no adverse impact on the adsorption capacity. The strong binding of SCBC-La with PO_4^{3-} is recognized as the dominating reason for the formation of inner-sphere complexes,[33] which endows SCBC-La with a unique capability of capturing PO_4^{3-}.

2.7. Removal of Low-Concentration Phosphate. In order to investigate if the United States Environmental Protection Agency (USEPA) standards for phosphate in wastewater can be satisfied by using SCBC-La as an adsorbent, adsorptive removal of phosphate at a low concentration was also studied. When exposed to 40 mL of an initial phosphate concentration of 2.0 mg L^{-1}, 50 mg of SCBC-La adsorbed 99.7% of the phosphate in solution after 2 h treatment (see Figure 8b). Importantly, the residual phosphate concentration in the solution is very low (7 μg L^{-1}), which can meet the USEPA standards for eutrophication prevention of <50 μg L^{-1} phosphate. In addition, the leaching concentration of La (0.002028 mg L^{-1}, Figure 8b) measured by inductively coupled plasma-mass spectroscopy (ICP-MS) is extremely low, indicating that lanthanum is not easily leached from SCBC-La. This indicates that $La(OH)_3$ nanoparticles may be stably immobilized on the surface of SCBC, probably due to the relatively strong interfacial affinity between them. The above tests indicated that the nanocomposite SCBC-La is a promising candidate with high efficiency for phosphate removal.

https://doi.org/10.1021/acsomega.3c00992
ACS Omega 2023, 8, 14177−14189

2.8. Desorption and Regeneration. In spite of many advantages including cost-effectiveness and highly efficient features, the used adsorbent should be able to be regenerated and recycled.[52] The desorption of phosphate from the exhausted adsorbents plays a key role in the regeneration of adsorbents. In general, the desorption of PO_4^{3-} from La-based materials is very difficult mostly because of the strong binding between La sites and PO_4^{3-}.[66] Hence, several harsh methods have been often employed to release the desorption, such as the treatment with 50−70% (12.5−17.5 M) NaOH solution at 140−150 °C for many hours. As shown in Figure S7, it is clear that both O═P−O bending and O−P−O bending peaks disappear when 5.0 M NaOH is used as the desorption medium, indicating that a relatively high NaOH concentration can facilitate the desorption of PO_4^{3-}. Meanwhile, Figure S8 compares the effect of three different temperatures (20, 60, and 100 °C) for 1.0 h by using 5.0 M NaOH on the adsorption performances of regenerated SCBC-La. The amounts of adsorbed phosphate are found to increase with increasing temperature of desorption, and the PO_4^{3-} adsorption capacity of SCBC-La can be nearly recovered to its original value when the desorption temperature is over 60 °C. After the recycle, the content of La decreased slightly and remained at roughly 92.69% of the original value at a desorption temperature of 60 °C (Figure S9), indicating that most of the La content in SCBC-La could be sustained after the adsorption−desorption process. Therefore, NaOH solution is an effective phosphate desorbent for SCBC-La. Based on the above results, it is indicated that the as-prepared SCBC-La exhibits good regeneration and reuse performance for phosphate adsorption.

3. CONCLUSIONS

In this work, a sustainable bioderived adsorbent (SCBC-La) has been successfully prepared from *S. canadensis via* a facile chemical precipitation process for highly effective and selective removal of phosphate. The as-obtained SCBC-La shows a high Brunauer−Emmett−Teller (BET) specific surface area (S_{BET}) of 55.87 $m^2\ g^{-1}$, 7 times that of SCBC and a high point of zero charge (~8.49). Benefitting from these features, the adsorption capacity of SCBC-La is boosted by 132-fold to 58.8 mg P g^{-1} compared with SCBC (0.44 mg P g^{-1}). The well-dispersed $La(OH)_3$ nanorods and highly positive charge are responsible for the excellent phosphate removal capability of SCBC-La and high anti-interference capability in terms of the pH value, coexisting ions, and ionic strength. Moreover, the reversible transformation between $La(OH)_3$ and $LaPO_4$ is manifested, and SCBC-La can be readily regenerated by treating with NaOH solution. Therefore, this work provides a facile approach to producing a novel high-performance biochar-based nanocomposite from an invasive plant (*S. canadensis*) for the effective removal of phosphate from water. Nevertheless, the pollutant composition in actual wastewater is often more complicated, and the research on enhancing pollutants removal by this kind of La-modified SCBC composite should be further studied.

4. EXPERIMENTAL SECTION

4.1. Materials. The above-ground biomass of a notorious invasive plant species (*S. canadensis*) in China was collected from Taizhou, Zhejiang Province, China. Lanthanum trichloride heptahydrate ($LaCl_3{\cdot}7H_2O$, AR), ammonium molybdate tetrahydrate ($(NH_4)_6Mo_7O_{24}{\cdot}4H_2O$, AR), and potassium antimonyl tartrate ($K(SbO)C_4H_6O_6{\cdot}0.5H_2O$, AR) were obtained from Aladdin Chemistry Co., Ltd. Potassium dihydrogen phosphate (KH_2PO_4, AR), potassium nitrate (KNO_3, AR), potassium sulfate (K_2SO_4, AR), potassium hydrogen carbonate ($KHCO_3$, AR), sodium chloride (NaCl, AR), potassium hydroxide (NaOH, AR), and hydrochloride acid (HCl, AR) were purchased from Sinopharm Chemical Reagent Co., Ltd. The stock phosphate solution of a concentration of 1000 mg L^{-1} (computed in P) was prepared by dissolving 4.3940 g of potassium dihydrogen phosphate into 1000 mL of deionized water, which would be further diluted with deionized water to the required concentrations of phosphate solutions.

4.2. Preparation of *S. canadensis*-Derived Biochar (SCBC). SCBC was obtained by an oxygen-limiting pyrolysis method as follows, and the pyrolysis experiment was carried out in a tube furnace (TL1200, Nanjing BYT Instrument Technology Co., LTD, China).[49] First, the leaves of *S. canadensis* were removed, and the remaining stems were dried and shattered to 100−200 mesh. Then, 5 g of *S. canadensis* powder was placed in a horizontal ceramic boat in the center of the furnace. Prior to the carbonization, the air was exhausted from the side of the quartz tube with the aid of a vacuum pump, and then, the high-purity N_2 was injected into the quartz tube at a gas flow of 300 mL min^{-1}. Finally, the furnace was heated to 700 °C with a ramping rate of 10° C min^{-1} for 2 h. After cooling to room temperature, *S. canadensis*-derived biochar (SCBC) was obtained. In addition, the yield of biochar was calculated based on the weight difference before and after pyrolysis, as given in eq 4.[67] The obtained biochar had a mass yield of 21.2 wt %.

$$\text{the yield of biochar (\%)} = \text{biochar mass (g)/biomass mass (g)} \times 100\% \quad (4)$$

4.3. Preparation of *S. canadensis*-Derived Biochar Nanocomposite (SCBC-La). SCBC-La was synthesized *via* a simple chemical precipitation approach as follows.[68] In brief, 2.0 g of SCBC was added into a 250 mL three-neck flask containing a 100 mL mixed solvent of deionized water and ethanol (v/v, 4/1) with at around 5 cm liquid depth, and the mixture was ultrasonicated for 10 min. 3.71 g of $LaCl_3{\cdot}7H_2O$ was then added into the former suspension and stirred for 2 h for adsorbing La^{3+} onto the surface of SCBC. Afterward, a certain amount of 1.0 M NaOH solution was subsequently added slowly dropwise within 2 h. The mixture solution was stirred for 2 h at 60 °C and continued to react at 25 °C for 12 h. The precipitate was collected by vacuum filtration. After drying at 60 °C for 24 h, *S. canadensis*-derived biochar-based nanocomposite (SCBC-La) was prepared. In addition, lanthanum hydroxide was synthesized by a conventional precipitation approach through the reaction between sodium hydroxide and lanthanum chloride.

4.4. Phosphate Adsorption. Adsorption isotherm experiments of PO_4^{3-} by SCBC-La were studied with varied initial phosphate concentrations ranging from 50 to 120 mg L^{-1} at a pH value of around 6.0. Batch experiments for phosphate adsorption were conducted in duplicate. Adsorption kinetic experiments were performed by exposing seventeen 50 mg samples of SCBC-La to 40 mL of an aqueous, 50 mg L^{-1} solution of PO_4^{3-} in a Teflon-lined screw-capped glass tube. Then, 1.5 mL of sample was taken out from each solution at predetermined time intervals. The solution pH effect on PO_4^{3-}

https://doi.org/10.1021/acsomega.3c00992
ACS Omega 2023, 8, 14177−14189

removal was determined. Typically, 50 mg of SCBC-La was put into a Teflon-lined screw-capped glass tube containing a 40 mL solution with 120 mg L^{-1} PO_4^{3-}, and 0.1 M NaOH or HCl was added to adjust the solution to the desired pH (3.0−9.0). The competing experiments were carried out involving the addition of typically present NO_3^-, SO_4^{2-}, and HCO_3^- anions at different concentrations (100, 200, and 300 mg L^{-1}). Various NaCl concentrations (0.01 and 0.1 M) were used to examine the effect of ionic strength on PO_4^{3-} removal by SCBC-La. At the end of each experiment, the solutions were separated by filtration using a 0.45 μm filter and then the residual phosphate ions were analyzed by UV−Vis spectrometry or ICP-MS. The residual phosphate concentration in the solution was calculated according to the molybdenum blue method on a T6 UV−Vis spectrophotometer (PUXI, China) at a detection wavelength of 700 nm. The adsorption capacity Q_e (mg g^{-1}) was obtained by eq 5

$$Q_e = (C_0 - C_e)V/m \quad (5)$$

where V (mL) and m (g) are, respectively, the volume of the phosphate solution and the dry weight of the used adsorbent mass. C_0 and C_e refer to the initial and equilibrium phosphate concentrations of the solution (mg L^{-1}), respectively.

4.5. Regeneration of Adsorbent. Adsorption−desorption experiments were performed to evaluate the reusability of SCBC-La according to the modification of a previous study.[33] First, SCBC-La was added into the phosphate solution, and then, the mixture solution was shaken in a constant temperature oscillation shaker for 48 h at 25 °C. Next, the used SCBC-La was regenerated at various concentrations (0.1, 0.5, 1, and 5 M) of NaOH solution at 60 °C for 1 h. After that, the regeneration characteristics were analyzed at different temperatures (20, 60, and 100 °C) with the concentration of NaOH at 5 M for 1 h. Then, the regenerated SCBC-La was washed to neutral using distilled water and collected to reuse.

4.6. Analysis and Characterization. The phosphate concentration was calculated using a UV−vis spectrophotometer (T6, Beijing Puxi Instrument Co., Beijing, China) and, for an extra low concentration (≤1.0 mg L^{-1}), by inductively coupled plasma-mass spectrometry (ICP-MS, Thermo Fisher Scientific Inc.). The pH was measured using a pH meter (FE20, METTLER TOLEDO Inc.), which was calibrated with standard buffer solutions. The microscopic morphology of the sample was examined using a scanning electron microscope (SEM, Hitachi S-4800, Tokyo, Japan). Prior to the test, the samples were gold-coated using an Ion Sputter Coater E1010 (Hitachi, Japan). Transmission electron microscopy (TEM) images were collected on a JEOL JEM-1230 transmission electron microscope (JEOL Ltd., Japan). The ζ-potential of each sample was determined using a Zetasizer Nano S90 (Malvern Instruments Ltd.). X-ray photoelectron spectroscopy (XPS) measurements were performed on an ESCALAB 250 X-ray photoelectron spectrometer (Thermo Fisher Scientific Inc.). The binding energy was calibrated by setting C 1s to 284.8 eV. The N_2 adsorption−desorption isotherms were obtained at 77 K with a MAC ASAP 2460 volumetric adsorption analyzer (MAC Instruments). Before measurement, each sample was treated by heating for 12 h at 105 °C. The specific surface area was calculated using the Brunauer−Emmett−Teller (BET) model, while the average pore size and the pore volume were evaluated by the adsorption branch of the isotherm and calculated using the Barrett−Joyner−Halenda (BJH) model. Infrared spectra of the samples were recorded utilizing KBr pellets on a Vector 22 FT-IR spectrometer (Bruker, Germany) in the range of 400−4000 cm^{-1}. Powder X-ray diffraction (XRD) data of the samples were characterized on a D8 Discover diffractometer (Bruker, AXS, Germany) using filtered Cu Kα radiation. The scanning range of diffraction angle (2θ) was 10−80°.

■ ASSOCIATED CONTENT

Supporting Information

The Supporting Information is available free of charge at https://pubs.acs.org/doi/10.1021/acsomega.3c00992.

XPS spectra of SCBC and SCBC-La (Figure S1); ζ-potential of SC, SCBC, and SCBC-La (Figure S2); dependence of adsorption efficiency on the initial phosphate concentration (Figure S3); Freundlich model for SCBC-La (Figure S4); Temkin model for SCBC-La (Figure S5); fitting results for pseudo-first-order models for SCBC-La (Figure S6); FT-IR spectra of fresh SCBC-La, SCBC-La after adsorption, and exhausted SCBC-La after desorption using different NaOH concentrations (Figure S7); the amount of adsorbed phosphate by SCBC-La when desorption was performed at three different temperatures (20, 60, and 100 °C) (b) (Figure S8); the lanthanum contents of SCBC-La and that after the recycle at three different temperatures (Figure S9); and comparison of phosphate adsorption on SCBC-La and some La composites (Table S1) (PDF)

■ AUTHOR INFORMATION

Corresponding Authors

Xiaohuan Liu − *College of Life Science, Zhejiang Provincial Key Laboratory of Plant Evolutionary Ecology and Conservation, Taizhou University, Taizhou 318000, P. R. China; School of Engineering, Zhejiang A&F University, Hangzhou 311300, P. R. China;* orcid.org/0000-0002-3402-8357; Email: liuxiaohuancaf@163.com, liuxh@tzc.edu.cn

Pingan Song − *Centre for Future Materials, University of Southern Queensland, Springfield 4350, Australia;* orcid.org/0000-0003-1082-652X; Email: pingan.song@usq.edu.au

Authors

Enmin Zong − *College of Life Science, Zhejiang Provincial Key Laboratory of Plant Evolutionary Ecology and Conservation, Taizhou University, Taizhou 318000, P. R. China; School of Earth Sciences and Engineering, Nanjing University, Nanjing 210093, P. R. China*

Yuanyuan Shen − *College of Life Science, Zhejiang Provincial Key Laboratory of Plant Evolutionary Ecology and Conservation, Taizhou University, Taizhou 318000, P. R. China*

Jiayao Yang − *School of Engineering, Zhejiang A&F University, Hangzhou 311300, P. R. China*

Complete contact information is available at: https://pubs.acs.org/10.1021/acsomega.3c00992

Notes

The authors declare no competing financial interest.

https://doi.org/10.1021/acsomega.3c00992
ACS Omega 2023, 8, 14177−14189

■ ACKNOWLEDGMENTS

This work was supported by the National Natural Science Foundation of China under Grant Nos. 22006111 and 21806142, the Zhejiang Provincial Natural Science Foundation of China under Grant No. LY20B070002, the Outstanding Youth Foundation of Taizhou University under Grant No. 2018YQ005, the China Postdoctoral Science Foundation under Grant No. 2019M661796, and Taizhou Science and Technology Planning Project under Grant No. 22hbb03. We would like to thank Dr. Jiang Wang for kindly proving raw materials, and Xianjun Liao for kindly helping on the preparation of composite.

■ REFERENCES

(1) Efome, J. E.; Rana, D.; Matsuura, T.; Lan, C. Q. Effects of operating parameters and coexisting ions on the efficiency of heavy metal ions removal by nano-fibrous metal-organic framework membrane filtration process. *Sci. Total. Environ.* **2019**, *674*, 355−362.

(2) Efome, J. E.; Rana, D.; Matsuura, T.; Lan, C. Q. Experiment and modeling for flux and permeate concentration of heavy metal ion in adsorptive membrane filtration using a metal-organic framework incorporated nanofibrous membrane. *Chem. Eng. J.* **2018**, *352*, 737−744.

(3) Liu, X.; Cheng, W.; Yu, Y.; Jiang, S.; Xu, Y.; Zong, E. Magnetic ZrO_2/PEI/Fe3O4 functionalized MWCNTs composite with enhanced phosphate removal performance and easy separability. *Composites, Part B* **2022**, *237*, 109861−109873.

(4) Efome, J. E.; Rana, D.; Matsuura, T.; Lan, C. Q. Insight Studies on Metal-Organic Framework Nanofibrous Membrane Adsorption and Activation for Heavy Metal Ions Removal from Aqueous Solution. *ACS Appl. Mater. Interfaces* **2018**, *10*, 18619−18629.

(5) Efome, J. E.; Rana, D.; Matsuura, T.; Lan, C. Q. Metal−organic frameworks supported on nanofibers to remove heavy metals. *J. Mater. Chem. A* **2018**, *6*, 4550−4555.

(6) Parvaresh, V.; Hashemi, H.; Khodabakhshi, A.; Sedehi, M. Removal of dye from synthetic textile wastewater using agricultural wastes and determination of adsorption isotherm. *Desalin. Water Treat.* **2018**, *111*, 345−350.

(7) Mirnasab, M. A.; Hashemi, H.; Samaei, M. R.; Azhdarpoor, A. Advanced removal of water NOM by Pre-ozonation, Enhanced coagulation and Bio-augmented Granular Activated Carbon. *Int. J. Environ. Sci. Technol.* **2021**, *18*, 3143−3152.

(8) Rookesh, T.; Samaei, M. R.; Yousefinejad, S.; Hashemi, H.; Derakhshan, Z.; Abbasi, F.; Jalili, M.; Giannakis, S.; Bilal, M. Investigating the Electrocoagulation Treatment of Landfill Leachate by Iron/Graphite Electrodes: Process Parameters and Efficacy Assessment. *Water* **2022**, *14*, 205.

(9) Nematolahia, S. Z.; Dehghanib, M.; Yousefinejadb, S.; Hashemic, H.; Golakic, M.; Mohammadpourc, A.; Abdollahid, S. H. Removal of metformin from aqueous solution using Fe^{3+} doped TiO. *Environment* **2021**, *8*, 182−189.

(10) Zong, E.; Fan, R.; Hua, H.; Yang, J.; Jiang, S.; Dai, J.; Liu, X.; Song, P. A magnetically recyclable lignin-based bio-adsorbent for efficient removal of Congo red from aqueous solution. *Int. J. Biol. Macromol.* **2023**, *226*, 443−453.

(11) Shan, X.; Yang, L.; Zhao, Y.; Yang, H.; Xiao, Z.; An, Q.; Zhai, S. Biochar/Mg-Al spinel carboxymethyl cellulose-La hydrogels with cationic polymeric layers for selective phosphate capture. *J. Colloid Interface Sci.* **2022**, *606*, 736−747.

(12) Yang, H.-R.; Li, S.-S.; Shan, X.-C.; Yang, C.; An, Q.-D.; Zhai, S.-R.; Xiao, Z.-Y. Hollow polyethyleneimine/carboxymethyl cellulose beads with abundant and accessible sorption sites for ultra-efficient chromium (VI) and phosphate removal. *Sep. Purif. Technol.* **2021**, *278*, No. 119607.

(13) Shan, X.; Zhao, Y.; Bo, S.; Yang, L.; Xiao, Z.; An, Q.; Zhai, S. Magnetic aminated lignin/CeO_2/Fe_3O_4 composites with tailored interfacial chemistry and affinity for selective phosphate removal. *Sci. Total Environ.* **2021**, *796*, No. 148984.

(14) Zhao, Y.; Gai, L.; Liu, H.; An, Q.; Xiao, Z.; Zhai, S. Network interior and surface engineering of alginate-based beads using sorption affinity component for enhanced phosphate capture. *Int. J. Biol. Macromol.* **2020**, *162*, 301−309.

(15) Zheng, D.; Yao, R.; Sun, C.; Zheng, Y.; Liu, C. Highly Efficient Low-Concentration Phosphate Removal from Effluents by Recoverable $La(OH)_3$/Foamed Nickel Adsorbent. *ACS Omega* **2021**, *6*, 5399−5407.

(16) Othman, A.; Dumitrescu, E.; Andreescu, D.; Andreescu, S. Nanoporous Sorbents for the Removal and Recovery of Phosphorus from Eutrophic Waters: Sustainability Challenges and Solutions. *ACS Sustainable Chem. Eng.* **2018**, *6*, 12542−12561.

(17) Gu, Y.; Xie, D.; Ma, Y.; Qin, W.; Zhang, H.; Wang, G.; Zhang, Y.; Zhao, H. Size Modulation of Zirconium-Based Metal Organic Frameworks for Highly Efficient Phosphate Remediation. *ACS Appl. Mater. Interfaces* **2017**, *9*, 32151−32160.

(18) Liu, T.; Zheng, S.; Yang, L. Magnetic zirconium-based metal−organic frameworks for selective phosphate adsorption from water. *J. Colloid Interface Sci.* **2019**, *552*, 134−141.

(19) Zhao, Y.; Guo, L.; Shen, W.; An, Q.; Xiao, Z.; Wang, H.; Cai, W.; Zhai, S.; Li, Z. Function integrated chitosan-based beads with throughout sorption sites and inherent diffusion network for efficient phosphate removal. *Carbohydr. Polym.* **2020**, *230*, No. 115639.

(20) Türker, M.; Çelen, I. Removal of ammonia as struvite from anaerobic digester effluents and recycling of magnesium and phosphate. *Bioresour. Technol.* **2007**, *98*, 1529−1534.

(21) Li, B.; Boiarkina, I.; Yu, W.; Huang, H. M.; Munir, T.; Wang, G. Q.; Young, B. R. Phosphorous recovery through struvite crystallization: Challenges for future design. *Sci. Total Environ.* **2019**, *648*, 1244−1256.

(22) Luo, X.; Liu, C.; Yuan, J.; Zhu, X.; Liu, S. Interfacial Solid-Phase Chemical Modification with Mannich Reaction and Fe(III) Chelation for Designing Lignin-Based Spherical Nanoparticle Adsorbents for Highly Efficient Removal of Low Concentration Phosphate from Water. *ACS Sustainable Chem. Eng.* **2017**, *5*, 6539−6547.

(23) Min, X.; Wu, X.; Shao, P.; Ren, Z.; Ding, L.; Luo, X. Ultra-high capacity of lanthanum-doped UiO-66 for phosphate capture: Unusual doping of lanthanum by the reduction of coordination number. *Chem. Eng. J.* **2019**, *358*, 321−330.

(24) Liao, T.; Li, T.; Su, X.; Yu, X.; Song, H.; Zhu, Y.; Zhang, Y. $La(OH)_3$-modified magnetic pineapple biochar as novel adsorbents for efficient phosphate removal. *Bioresour. Technol.* **2018**, *263*, 207−213.

(25) Zong, E.; Liu, X.; Jiang, J.; Fu, S.; Chu, F. Preparation and characterization of zirconia-loaded lignocellulosic butanol residue as a biosorbent for phosphate removal from aqueous solution. *Appl. Surf. Sci.* **2016**, *387*, 419−430.

(26) Tanada, S.; Kabayama, M.; Kawasaki, N.; Sakiyama, T.; Nakamura, T.; Araki, M.; Tamura, T. Removal of phosphate by aluminum oxide hydroxide. *J. Colloid Interface Sci.* **2003**, *257*, 135−140.

(27) Liu, X.; He, X.; Zhang, J.; Yang, J.; Xiang, X.; Ma, Z.; Liu, L.; Zong, E. Cerium oxide nanoparticle functionalized lignin as a nano-biosorbent for efficient phosphate removal. *RSC Adv.* **2020**, *10*, 1249−1260.

(28) Peiris, C.; Gunatilake, S. R.; Mlsna, T. E.; Mohan, D.; Vithanage, M. Biochar based removal of antibiotic sulfonamides and tetracyclines in aquatic environments: A critical review. *Bioresour. Technol.* **2017**, *246*, 150−159.

(29) Li, G.; Zhu, W.; Zhang, C.; Zhang, S.; Liu, L.; Zhu, L.; Zhao, W. Effect of a magnetic field on the adsorptive removal of methylene blue onto wheat straw biochar. *Bioresour. Technol.* **2016**, *206*, 16−22.

(30) Li, R.; Deng, H.; Zhang, X.; Wang, J. J.; Awasthi, M. K.; Wang, Q.; Xiao, R.; Zhou, B.; Du, J.; Zhang, Z. High-efficiency removal of Pb(II) and humate by a CeO_2−MoS_2 hybrid magnetic biochar. *Bioresour. Technol.* **2019**, *273*, 335−340.

https://doi.org/10.1021/acsomega.3c00992
ACS Omega 2023, 8, 14177−14189

(31) Wang, Z.; Shen, D.; Shen, F.; Li, T. Phosphate adsorption on lanthanum loaded biochar. *Chemosphere* **2016**, *150*, 1−7.
(32) Tan, X.-f.; Liu, Y.-g.; Gu, Y.-l.; Xu, Y.; Zeng, G.-m.; Hu, X.-j.; Liu, S.-b.; Wang, X.; Liu, S.-m.; Li, J. Biochar-based nano-composites for the decontamination of wastewater: A review. *Bioresour. Technol.* **2016**, *212*, 318−333.
(33) Liu, X.; Zong, E.; Hu, W.; Song, P.; Wang, J.; Liu, Q.; Ma, Z.; Fu, S. Lignin-Derived Porous Carbon Loaded with $La(OH)_3$ Nanorods for Highly Efficient Removal of Phosphate. *ACS Sustainable Chem. Eng.* **2019**, *7*, 758−768.
(34) Liu, L.; Zhang, C.; Chen, S.; Ma, L.; Li, Y.; Lu, Y. Phosphate adsorption characteristics of $La(OH)_3$-modified, canna-derived biochar. *Chemosphere* **2022**, *286*, No. 131773.
(35) Chen, L.; Liu, F.; Wu, Y.; Zhao, L.; Li, Y.; Zhang, X.; Qian, J. In situ formation of $La(OH)_3$-poly(vinylidene fluoride) composite filtration membrane with superior phosphate removal properties. *Chem. Eng. J.* **2018**, *347*, 695−702.
(36) Zhang, Y.; Pan, B.; Shan, C.; Gao, X. Enhanced Phosphate Removal by Nanosized Hydrated La(III) Oxide Confined in Cross-linked Polystyrene Networks. *Environ. Sci. Technol.* **2016**, *50*, 1447−1454.
(37) Zhao, S. Y.; Sun, S.; Dai, C.; Gituru, R.; Chen, J.; Wang, Q. Genetic variation and structure in native and invasive S olidago canadensis populations. *Weed Res.* **2015**, *55*, 163−172.
(38) Rajapaksha, A. U.; Vithanage, M.; Lim, J. E.; Ahmed, M. B. M.; Zhang, M.; Lee, S. S.; Ok, Y. S. Invasive plant-derived biochar inhibits sulfamethazine uptake by lettuce in soil. *Chemosphere* **2014**, *111*, 500−504.
(39) Ahmad, M.; Moon, D. H.; Vithanage, M.; Koutsospyros, A.; Lee, S. S.; Yang, J. E.; Lee, S. E.; Jeon, C.; Ok, Y. S. Production and use of biochar from buffalo-weed (Ambrosia trifida L.) for trichloroethylene removal from water. *J. Chem. Technol. Biotechnol.* **2014**, *89*, 150−157.
(40) Vithanage, M.; Rajapaksha, A. U.; Tang, X.; Thiele-Bruhn, S.; Kim, K. H.; Lee, S.-E.; Ok, Y. S. Sorption and transport of sulfamethazine in agricultural soils amended with invasive-plant-derived biochar. *J. Environ. Manage.* **2014**, *141*, 95−103.
(41) Rajapaksha, A. U.; Vithanage, M.; Ahmad, M.; Seo, D.-C.; Cho, J.-S.; Lee, S.-E.; Lee, S. S.; Ok, Y. S. Enhanced sulfamethazine removal by steam-activated invasive plant-derived biochar. *J. Hazard. Mater.* **2015**, *290*, 43−50.
(42) Zhang, Z.; Chen, L.; Wang, J.; Yao, J.; Li, J. Biochar preparation from *Solidago canadensis* and its alleviation of the inhibition of tomato seed germination by allelochemicals. *RSC Adv.* **2018**, *8*, 22370−22375.
(43) Dong, L.; Li, S.; Jin, Y.; Hu, B.; Sheng, G. Enhanced adsorption of Eu(III) from wastewater using *Solidago canadensis*-derived biochar functionalized by Ca/Al-LDH and hydroxyapatite. *Appl. Surf. Sci.* **2021**, *567*, No. 150794.
(44) Lian, W.; Yang, L.; Joseph, S.; Shi, W.; Bian, R.; Zheng, J.; Li, L.; Shan, S.; Pan, G. Utilization of biochar produced from invasive plant species to efficiently adsorb Cd (II) and Pb (II). *Bioresour. Technol.* **2020**, *317*, No. 124011.
(45) Zhang, L.; Cheng, H.; Pan, D.; Wu, Y.; Ji, R.; Li, W.; Jiang, X.; Han, J. One-pot pyrolysis of a typical invasive plant into nitrogen-doped biochars for efficient sorption of phthalate esters from aqueous solution. *Chemosphere* **2021**, *280*, No. 130712.
(46) Rana, D.; Bag, K.; Bhattacharyya, S.; Mandal, B. Miscibility of poly (styrene-co-butyl acrylate) with poly (ethyl methacrylate): Existence of both UCST and LCST. *J. Polym. Sci., Part B: Polym. Phys.* **2000**, *38*, 369−375.
(47) Rana, D.; Mandal, B.; Bhattacharyya, S. Analogue calorimetric studies of blends of poly (vinyl ester) s and polyacrylates. *Macromolecules* **1996**, *29*, 1579−1583.
(48) Rana, D.; Mandal, B.; Bhattacharyya, S. Analogue calorimetry of polymer blends: poly (styrene-co-acrylonitrile) and poly (phenyl acrylate) or poly (vinyl benzoate). *Polymer* **1996**, *37*, 2439−2443.
(49) Ma, Z.; Yang, Y.; Ma, Q.; Zhou, H.; Luo, X.; Liu, X.; Wang, S. Evolution of the chemical composition, functional group, pore structure and crystallographic structure of bio-char from palm kernel shell pyrolysis under different temperatures. *J. Anal. Appl. Pyrolysis* **2017**, *127*, 350−359.
(50) He, J.; Wang, W.; Sun, F.; Shi, W.; Qi, D.; Wang, K.; Shi, R.; Cui, F.; Wang, C.; Chen, X. Highly Efficient Phosphate Scavenger Based on Well-Dispersed $La(OH)_3$ Nanorods in Polyacrylonitrile Nanofibers for Nutrient-Starvation Antibacteria. *ACS Nano* **2015**, *9*, 9292−9302.
(51) Zong, E.; Wang, C.; Yang, J.; Zhu, H.; Jiang, S.; Liu, X.; Song, P. Preparation of TiO_2/cellulose nanocomposites as antibacterial bio-adsorbents for effective phosphate removal from aqueous medium. *Int. J. Biol. Macromol.* **2021**, *182*, 434−444.
(52) Kim, M.; Kim, H.; Byeon, S.-H. Layered Yttrium Hydroxide l-$Y(OH)_3$ Luminescent Adsorbent for Detection and Recovery of Phosphate from Water over a Wide pH Range. *ACS Appl. Mater. Interfaces* **2017**, *9*, 40461−40470.
(53) Zhang, L.; Zhou, Q.; Liu, J.; Chang, N.; Wan, L.; Chen, J. Phosphate adsorption on lanthanum hydroxide-doped activated carbon fiber. *Chem. Eng. J.* **2012**, *185*−*186*, 160−167.
(54) Koilraj, P.; Sasaki, K. Selective removal of phosphate using La-porous carbon composites from aqueous solutions: Batch and column studies. *Chem. Eng. J.* **2017**, *317*, 1059−1068.
(55) Zhang, J.; Shen, Z.; Shan, W.; Chen, Z.; Mei, Z.; Lei, Y.; Wang, W. Adsorption behavior of phosphate on Lanthanum(III) doped mesoporous silicates material. *J. Environ. Sci.* **2010**, *22*, 507−511.
(56) Huang, W.; Zhu, Y.; Tang, J.; Yu, X.; Wang, X.; Li, D.; Zhang, Y. SI for Lanthanum-doped ordered mesoporous hollow silica spheres as novel adsorbents for efficient phosphate removal. *J. Mater. Chem. A* **2014**, *2*, 8839−8848.
(57) Yang, J.; Yuan, P.; Chen, H.-Y.; Zou, J.; Yuan, Z.; Yu, C. Rationally designed functional macroporous materials as new adsorbents for efficient phosphorus removal. *J. Mater. Chem.* **2012**, *22*, 9983−9990.
(58) Yang, J.; Zhou, L.; Zhao, L.; Zhang, H.; Yin, J.; Wei, G.; Qian, K.; Wang, Y.; Yu, C. A designed nanoporous material for phosphate removal with high efficiency. *J. Mater. Chem.* **2011**, *21*, 2489−2494.
(59) Li, Z.; Xiao, D.; Ge, Y.; Koehler, S. Surface-Functionalized Porous Lignin for Fast and Efficient Lead Removal from Aqueous Solution. *ACS Appl. Mater. Interfaces* **2015**, *7*, 15000−15009.
(60) Fang, L.; Shi, Q.; Nguyen, J.; Wu, B.; Wang, Z.; Lo, I. M. C. Removal Mechanisms of Phosphate by Lanthanum Hydroxide Nanorods: Investigations using EXAFS, ATR-FTIR, DFT, and Surface Complexation Modeling Approaches. *Environ. Sci. Technol.* **2017**, *51*, 12377−12384.
(61) Tang, Q.; Shi, C.; Shi, W.; Huang, X.; Ye, Y.; Jiang, W.; Kang, J.; Liu, D.; Ren, Y.; Li, D. Preferable phosphate removal by nano-La(III) hydroxides modified mesoporous rice husk biochars: Role of the host pore structure and point of zero charge. *Sci. Total Environ.* **2019**, *662*, 511−520.
(62) Li, M.; Zhang, L.; Fan, X.; Wu, M.; Wang, M.; Cheng, R.; Zhang, L.; Yao, H.; Shi, J. Core-shell $LaPO_4$/g-C_3N_4 nanowires for highly active and selective CO_2 reduction. *Appl. Catal., B* **2017**, *201*, 629−635.
(63) Zong, E.; Liu, X.; Wang, J.; Yang, S.; Jiang, J.; Fu, S. Facile preparation and characterization of lanthanum-loaded carboxylated multi-walled carbon nanotubes and their application for the adsorption of phosphate ions. *J. Mater. Sci.* **2017**, *52*, 7294−7310.
(64) Lü, J.; Liu, H.; Liu, R.; Zhao, X.; Sun, L.; Qu, J. Adsorptive removal of phosphate by a nanostructured Fe−Al−Mn trimetal oxide adsorbent. *Powder Technol.* **2013**, *233*, 146−154.
(65) Zong, E.; Guo, B.; Yang, J.; Shi, C.; Jiang, S.; Ma, Z.; Liu, X. Reusable Hyperbranched Polyethylenimine-Functionalized Ethyl Cellulose Film for the Removal of Phosphate with Easy Separation. *ACS Omega* **2021**, *6*, 505−515.
(66) Zhang, X.; Sun, F.; He, J.; Xu, H.; Cui, F.; Wang, W. Robust phosphate capture over inorganic adsorbents derived from lanthanum metal organic frameworks. *Chem. Eng. J.* **2017**, *326*, 1086−1094.
(67) Teh, Y. Y.; Lee, K. T.; Chen, W.-H.; Lin, S.-C.; Sheen, H.-K.; Tan, I. S. Dilute sulfuric acid hydrolysis of red macroalgae Eucheuma

https://doi.org/10.1021/acsomega.3c00992
ACS Omega 2023, 8, 14177−14189

denticulatum with microwave-assisted heating for biochar production and sugar recovery. *Bioresour. Technol.* **2017**, *246*, 20−27.
(68) Zong, E.; Huang, G.; Liu, X.; Lei, W.; Jiang, S.; Ma, Z.; Wang, J.; Song, P. A lignin-based nano-adsorbent for superfast and highly selective removal of phosphate. *J. Mater. Chem. A* **2018**, *6*, 9971−9983.

https://doi.org/10.1021/acsomega.3c00992
ACS Omega 2023, 8, 14177−14189